JOURNAL OF SOLID STATE CHEMISTRY 105, 428–433 (1993)

High-Pressure Synthesis, Crystal Structure, and Magnetic Properties of $Mn_{1-x}T_xGe_4$ (*T*: Co, Fe)

H. TAKIZAWA, K. YAMAZAKI, T. ENDO, AND M. SHIMADA

Department of Molecular Chemistry and Engineering, Faculty of Engineering, Tohoku University, Aoba-ku, Sendai, Miyagi 980, Japan

Received February 20, 1992; in revised form December 22, 1992; accepted December 29, 1992

$Mn_{1-x}T_xGe_4$ (*T*: Co, Fe) solid solution was synthesized at 6 GPa and 650–750°C using a belt-type high-pressure apparatus. The crystal structure of the $Mn_{1-x}T_xGe_4$ solid solution is related to the β-$NiHg_4$ type. The following structural changes were observed in the $Mn_{1-x}Co_xGe_4$ system: tetragonal ($x = 0$) to orthorhombic ($0 < x < 0.2$) and orthorhombic to pseudotetragonal ($0.2 \leqq x \leqq 0.4$). Similar structural changes were also observed at $0 < x < 0.4$ (tetra. → ortho.) and $x = 0.4$ (ortho.→ pseudotetra.) in the $Mn_{1-x}Fe_xGe_4$ system. These results indicate that the structural changes in $Mn_{1-x}T_xGe_4$ strongly depend on the average valence electron number of the transition metal atoms. $Mn_{1-x}T_xGe_4$ solid solutions are itinerant electron ferromagnets and the Curie temperature decreases linearly with decreasing unit-cell volume.

Introduction

In the binary transition metal(*T*)–metalloid atom(*X*) system, a large number of intermetallic compounds have been synthesized. These intermetallic compounds have various chemical compositions such as T_3X, T_2X, T_5X_3, TX, TX_2, T_3X_7, and TX_4(*1*, *2*). The compounds containing less than 67 at.% *X* atom are commonly formed in borides, silicides, germanides, and pnictides, while TX_4 compounds are mainly formed in borides and pnictides, and rarely in silicides and germanides.

Recently, two new germanides, $MnGe_4$ and $CoGe_4$, were synthesized under high-pressure/temperature conditions (*3*). The crystal structures of $MnGe_4$ and $CoGe_4$ are closely related to the β-$NiHg_4$-type structure; the unit cell of $MnGe_4$ is composed of four β-$NiHg_4$-type cells and that of $CoGe_4$ is composed of eight β-$NiHg_4$-type cells. $MnGe_4$ behaves like an itinerant-electron ferromagnet with a Curie temperature of 340 K. $CoGe_4$ is a Pauli paramagnetic metal.

In the present study, $Mn_{1-x}Co_xGe_4$ solid solutions were synthesized under high-pressure/temperature conditions, and their magnetic properties were investigated. $Mn_{1-x}Fe_xGe_4$ solid solutions were also synthesized and characterized in order to clarify the influence of 3*d* electrons on crystal structure and magnetic properties.

Experimental

Manganese, cobalt, iron powders (>99.9% purity), and germanium powder (>99.99% purity) were used as starting materials. These powders were mixed in the atomic ratio $Ge/(Mn_{1-x}T_x) = 4.5$ (*T*: Co, Fe) and uniaxially pressed at 100 MPa to form a pellet; the excess of germanium was added to prevent the formation of germanide phases with lower germanium contents. The pellet was put into a cylindrical BN capsule, which was placed in a carbon heater. The assemblage was put into a cell constructed with NaCl and subjected to high-pressure/temperature conditions using a belt-type high-pressure apparatus. The high-pres-

0022-4596/93 $5.00

sure/temperature treatment was carried out at 6 GPa and 650–750°C for 2 hr, and then the sample was quenched to room temperature prior to the release of the applied pressure. The high-pressure reaction was repeated several times to obtain a well homogenized single-phase sample.

The pellet thus obtained was pulverized and the residual germanium was removed by leaching with 5*N* NaOH + 3% H_2O_2 solutions at room temperature.

The resulting phase was identified by X-ray powder diffraction analysis using Ni-filtered Cu$K\alpha$ radiation. Lattice parameters were determined by a least-squares method using silicon (a = 0.543088 nm) as an internal standard.

Magnetization and magnetic susceptibility were measured by a magnetic torsion balance in a magnetic field of up to 10 kOe in the temperature range 77–520 K.

Results and Discussion

1. High-Pressure Synthesis and Crystal Structure

$Mn_{1-x}Co_xGe_4$ solid solutions were synthesized under 6 GPa and 700°C for 2 hr. Single-phase solid solutions were obtained in the composition range $0 \leqq x \leqq 0.4$ and $0.7 \leqq x \leqq 1$. The X-ray powder diffraction patterns of the solid solutions were completely indexed based on β-$NiHg_4$-related superstructures as indicated in Ref. (*3*). The unit cell is composed of four β-$NiHg_4$-type cells ($a \approx b \approx 2c \approx 2a_0$) in the composition range $0 \leqq x \leqq 0.4$ and eight β-$NiHg_4$-type cells ($a = b = c = 2a_0$) in the range $0.7 \leqq x \leqq 1$, where a_0 is the unit cell parameter of cubic β-$NiHg_4$-type cell.

Figure 1 shows the variations of the lattice parameters in the $Mn_{1-x}Co_xGe_4$ system. The crystal structure of $MnGe_4$ is body-centered tetragonal with lattice parameters a = 1.103(1) nm and c = 0.5598(3) nm (*3*). The unit cell is orthorhombically distorted ($2c > a > b$) in the composition range $0 \leqq x < 0.2$, and pseudotetragonal ($2c = a > b$) in the composition range $0.2 \leqq x \leqq 0.4$. In the Co-rich region ($0.7 \leqq x \leqq 1$), the alloy is isostructural with cubic $CoGe_4$. All attempts to prepare single-phase solid solutions in the composition range $0.4 < x < 0.7$ resulted in mixtures of pseudotetragonal and cubic phases.

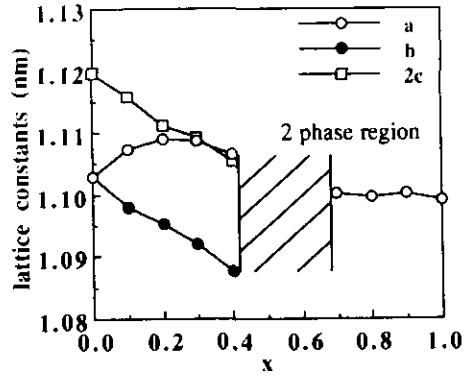

FIG. 1. Compositional dependence of lattice parameters in the system $Mn_{1-x}Co_xGe_4$.

$Mn_{1-x}Fe_xGe_4$ solid solutions were synthesized under 6 GPa and 700–750°C for 2 hr. Their X-ray powder diffraction patterns were completely indexed based on a β-$NiHg_4$-related type structure in the composition range $0 \leqq x \leqq 0.4$. In the composition range $x > 0.4$, the products were mixtures of $Mn_{0.6}Fe_{0.4}Ge_4$, $FeGe_2$, and Ge.

The crystal structure of $Mn_{1-x}Fe_xGe_4$ changed with iron concentration in a manner similar to the structure of the $Mn_{1-x}Co_xGe_4$ system; the unit cell was orthorhombic in the composition range $0 < x < 0.4$, and pseudotetragonal at $x = 0.4$.

Figure 2 shows the lattice constants of $Mn_{1-x}T_xGe_4$ (*T*: Co, Fe) solid solutions plotted against the average valence electron ($3d + 4s$) number per transition-metal atom. It is notable that the variation of the lattice parameters in both solid solution systems are quite similar and the structural change occurs at an isoelectronic composition. Such structural changes also occur in Mg-based pseudobinary alloys with the Laves structure (*4–6*). It was reported that the stabilization of various stacking variants in Laves phases strongly depends on the elec-

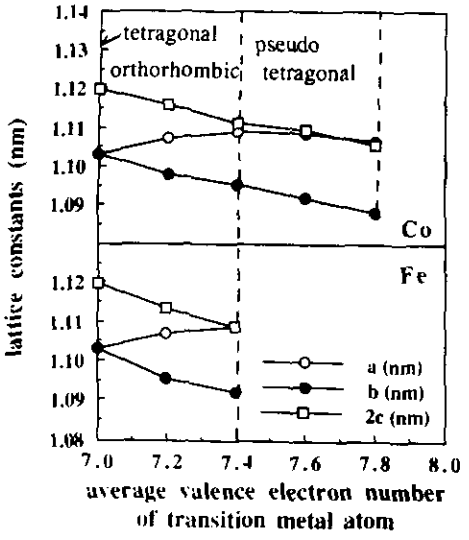

FIG. 2. Relation between lattice constants and average valence electron number of transition metal atoms of $Mn_{1-x}T_xGe_4$ (T: Co, Fe).

tron concentration of the constituent elements (6). Similarly, the present results shown in Fig. 2 suggest that the crystal structure of $Mn_{1-x}T_xGe_4$ is controlled by the 3*d* electron concentration, which indicates that the itinerant character of the 3*d* electrons plays an important role in determining the magnetic properties in $Mn_{1-x}T_xGe_4$, as discussed in the next section.

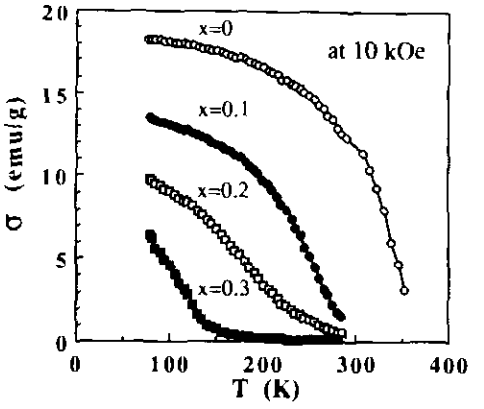

FIG. 4. Temperature dependence of the magnetization of $Mn_{1-x}Co_xGe_4$.

2. *Magnetic Properties*

The results of the magnetic measurements for the $Mn_{1-x}T_xGe_4$ (T: Co, Fe) systems are shown in Figs. 3–8. $Mn_{1-x}T_xGe_4$ solid solutions exhibit a ferromagnetic behavior. The saturation magnetization and the Curie temperature monotonically decrease with increasing content of the substituent metal.

Above the Curie temperature, the magnetic susceptibility follows the Curie–Weiss-type relation $M\chi_g = M\chi_c + C/(T - \theta_p)$, where M is the formula weight and χ_c is the temperature-independent magnetic susceptibility.

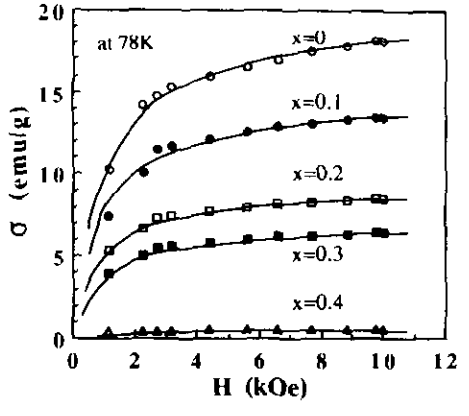

FIG. 3. Magnetic field dependence of the magnetization of $Mn_{1-x}Co_xGe_4$ (at 78 K).

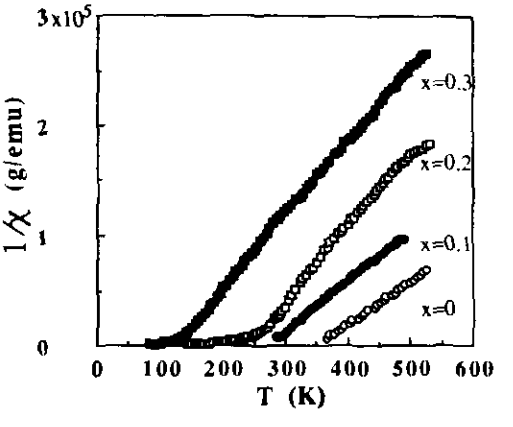

FIG. 5. Temperature dependence of the reciprocal magnetic susceptibility of $Mn_{1-x}Co_xGe_4$.

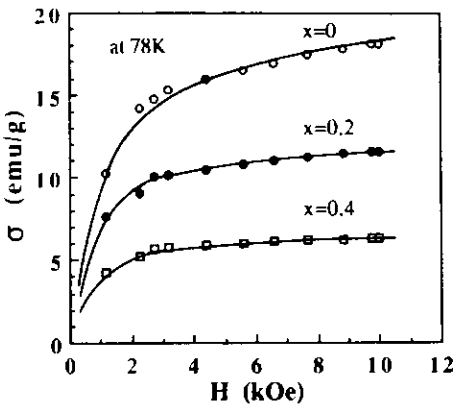

FIG. 6. Magnetic field dependence of the magnetization of $Mn_{1-x}Fe_xGe_4$ (at 78 K).

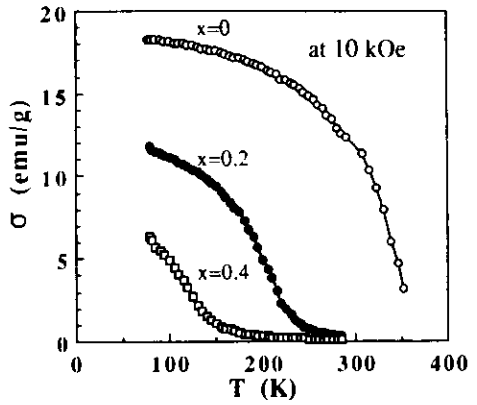

FIG. 7. Temperature dependence of the magnetization of $Mn_{1-x}Fe_xGe_4$.

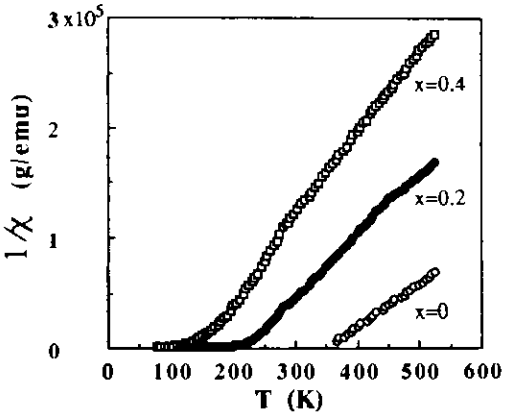

FIG. 8. Temperature dependence of the reciprocal magnetic susceptibility of $Mn_{1-x}Fe_xGe_4$.

The magnetic parameters of $Mn_{1-x}T_xGe_4$ are listed in Table I. Here, μ_c is the paramagnetic moment deduced from the following relation: $P_{eff}^2 = \mu_c(\mu_c + 2)$ (*7*). The ratio μ_c/μ_s (Rhodes–Wohlfarth ratio) (*7*, *8*), which is the criterion for itinerancy of the *d*-electrons, is also given in Table I. The μ_c/μ_s ratio of $Mn_{1-x}T_xGe_4$ is larger than unity and the value increases with decreasing Curie temperature. Such tendency is a common feature of itinerant-electron ferromagnet systems (*8*). It is generally known that the μ_c/μ_s ratio is equal to unity in ferromagnets with the localized magnetic moment systems. From these results, it is concluded that the 3d electrons in $Mn_{1-x}T_xGe_4$ exhibit itinerant character.

TABLE I

MAGNETIC PARAMETERS OF $Mn_{1-x}T_xGe_4$ (*T*: Co, Fe)

x	μ_s (μ_B)	P_{eff}(μ_B)	μ_c (μ_B)	μ_c/μ_s	T_C(K)	θ_p (K)
			T= Co			
0	1.2	2.83	2.00	1.7	340	348
0.1	0.87	2.35	1.55	1.7	270	273
0.2	0.62	1.90	1.15	1.85	230	247
0.3	(0.43)	2.02	1.25	(2.91)	140	124
			T = Fe			
0.2	0.77	2.23	1.45	1.88	210	218
0.4	(0.43)	1.83	1.09	(2.51)	120	152

Note. μ_s: saturation magnetic moment; P_{eff}: number of effective Bohr magneton; μ_c: paramagnetic moment.

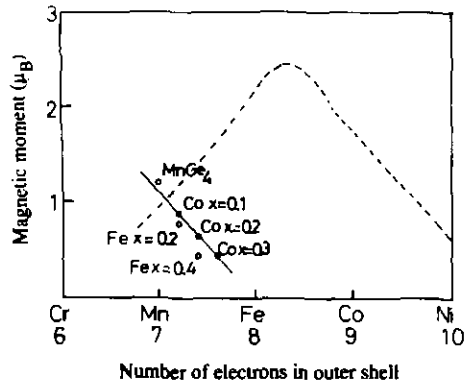

FIG. 9. Magnetic moment per transition metal atom as a function of the number of electrons in the outer shell for $Mn_{1-x}T_xGe_4$ (*T*: Co, Fe). The dotted line corresponds to the Slater–Pauling curve for 3*d* metals and alloys.

The saturation magnetic moments (μ_s) of $Mn_{1-x}T_xGe_4$ are plotted in Fig. 9 as a function of the number of $3d + 4s$ electrons per transition metal atom. The dotted line corresponds to the Slater–Pauling curve for 3*d* transition metals and alloys. The magnetic moment of $Mn_{1-x}T_xGe_4$ changes with electron concentration by the ratio of $1\mu_B$/electron, in a manner similar to the right-hand part of the Slater–Pauling curve. The data points of the magnetic moment vs electron number curve for the $Mn_{1-x}T_XGe_4$ system strongly shift to the left-hand side from those of 3*d* metals and alloys. The magnitude of the shift is equivalent to 2.5 electrons. This shift can be explained if we assume that germanium atoms donate 2.5 electrons (about 0.6 electrons per each germanium atom) to the 3*d* band of the transition metal atoms in $Mn_{1-x}T_xGe_4$.

A similar electron transfer was observed in transition-metal borides, T_2B, *TB*, TB_2 (*9, 10*), and germanides, *T*Ge (*11*). In the boride systems, each boron atom contributes about 1.7–1.8 electrons to the 3*d* band of the transition metal atom (*10*). This electron contribution is independent of crystal structure and chemical composition. In contrast, electron contributions strongly vary in the transition-metal/germanide systems: 0.7–1 electrons/germanium in *T*Ge with the B20 structure (*11*), 4 electrons/germanium in $TGe_{1.25}$–$TGe_{1.82}$ with the defect-disilicide-type structure (*12–14*), and 0.6 electrons/germanium in $Mn_{1-x}T_xGe_4$. Such differences may be due to the difference in bond nature originated in the metalloid character of germanium atom.

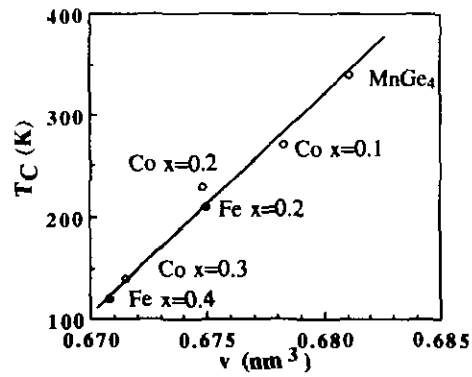

FIG. 10. Curie temperature of $Mn_{1-x}T_xGe_4$ (*T*: Co, Fe) as a function of the unit-cell volume.

Figure 10 shows the relation between Curie temperature and unit-cell volume of $Mn_{1-x}T_xGe_4$. The Curie temperature decreases linearly with decreasing unit-cell volume; that is, the ferromagnetic interaction strongly depends on the overlapping of 3*d* orbitals. This behavior is compatible with the fact that the ferromagnetism in metals, alloys, or intermetallic compounds is mainly explained by direct exchange interaction, as demonstrated by the Slater–Bethe curve (*15*).

Acknowledgment

This work has been supported in part by a Grant-in-Aid for Cooperative Research (A) on Survey of New Inorganic Materials and Synthetic Process of the Ministry of Education, Science and Culture.

References

1. P. ECKERLIN AND H. KANDLER, "Structure Data of Elements and Intermetallic Phases," Landolt-Börnstein Numerical Data and Functional Relationships in Science and Technology, New Series Group 3: Crystal and Solid State Physics (K. H.

Hellwege and A. M. Hellwege, Eds.), Vol. 6, Springer-Verlag, Berlin/Heidelberg/New York (1971).
2. B. Aronsson, T. Lundström, and S. Rundqvist, "Borides, Silicides and Phosphides," Methuen, London (1965).
3. H. Takizawa, T. Sato, T. Endo, and M. Shimada, *J. Solid State Chem.* **88,** 384 (1990).
4. R. L. Berry and G. V. Raynor, *Acta Crystallogr.* **6,** 178 (1953).
5. Y. Komura, *Acta Crystallogr.* **15,** 770 (1962).
6. Y. Komura and Y. Kitano, *Acta Crystallogr. Sect. B* **33,** 2496 (1977).
7. E. P. Wohlfarth, *J. Magn. Magn. Mater.*, **7,** 113 (1978).
8. P. Rhodes and E. P. Wohlfarth, *Proc. R. Soc. London Ser. A* **273,** 247 (1963).
9. J. Friedel, *in* "Phase Stability in Metals and Alloys" (P. S. Rudman, J. Stringer, and R. I. Jaffee, Eds.), pp. 353–354, McGraw–Hill, New York (1966).
10. M. C. Cadeville, *J. Phys. Chem. Solids* **27,** 667 (1966).
11. H. Takizawa, T. Sato, T. Endo, and M. Shimada, *J. Solid State Chem.* **73,** 40 (1988).
12. W. B. Pearson, *Acta Crystallogr. Sect. B* **26,** 1044 (1970).
13. W. Jeitschko and E. Parthé, *Acta Crystallogr.* **22,** 417 (1967).
14. H. Takizawa, T. Sato, T. Endo, and M. Shimada, *J. Solid State Chem.* **73,** 427 (1988).
15. A. Sommerfeld and H. A. Bethe, Ferromagnetism, *in* "Handbuch der Physik" (S. Flügge, Ed.), Vol. 24, Part II, pp. 595, Verlag Julius Springer, Berlin (1933).